Published in final edited form as:
Nature. 2016 August 4; 536(7614): 104–107. doi:10.1038/nature18966.

Structure of the adenosine A_{2A} receptor bound to an engineered G protein

Byron Carpenter[*], **Rony Nehmé**, **Tony Warne**, **Andrew G. W. Leslie**, and **Christopher G. Tate**[*]
MRC Laboratory of Molecular Biology, Francis Crick Avenue, Cambridge CB2 0QH, UK

G protein-coupled receptors (GPCRs) are essential components of the signalling network throughout the body. To understand the molecular mechanism of G protein-mediated signalling, structures of receptors are necessary in inactive conformations and in the active conformation coupled to a G protein1,2. Here we present the structure of the adenosine A_{2A} receptor ($A_{2A}R$) bound to an engineered G protein3, mini-G_s, to 3.4 Å resolution. Mini-G_s binds to $A_{2A}R$ through an extensive interface (1048 $Å^2$) that is similar, but not identical, to the interface between the β_2-adrenergic receptor (β_2AR) and G_s4. The transition of the receptor from an agonist-bound active-intermediate state5,6 to an active G protein-bound state is characterised by a 14 Å shift of the cytoplasmic end of transmembrane helix 6 (H6) away from the receptor core, slight changes in the positions of the cytoplasmic ends of H5 and H7 and rotamer changes of the amino acid side chains $Arg^{3.50}$, $Tyr^{5.58}$ and $Tyr^{7.53}$. There are no significant differences in the extracellular half of the receptor around the ligand binding pocket. The $A_{2A}R$–mini-G_s structure highlights both the diversity and similarity in G protein coupling to GPCRs7 and hints at the potential complexity of the molecular basis for G protein specificity.

Structures of $A_{2A}R$ bound to either inverse agonists8–10 or agonists5,6,11 have elucidated the molecular determinants of subtype specificity and ligand efficacy12. However, the mechanism of activation of the receptor to allow G protein coupling and the basis of G protein selectivity is not fully understood. Structures of $A_{2A}R$ in the inactive state have been determined bound either to the antagonists ZM2413858–10, XAC8, caffeine8 or 1,2,4-triazines13, and all the structures are very similar. An intramembrane Na^+ ion that can act as an allosteric antagonist was identified in the highest resolution structure (1.8 Å)14, and a homologous Na^+ ion has been subsequently identified in other high-resolution structures of GPCRs15–17. Four agonist-bound structures of $A_{2A}R$ have also been determined after co-crystallisation with either adenosine5, NECA5, CGS2168011 or UK4320976. All the

[*]Correspondence for the manuscript: Dr. C.G. Tate, MRC Laboratory of Molecular Biology, Francis Crick Avenue, Cambridge CB2 0QH, UK, cgt@mrc-lmb.cam.ac.uk, Telephone +44-(0)1223-267073.

Author contributions. B.C. performed receptor expression, purification, crystallization, cryo-cooling of the crystals, data collection, data processing and structure refinement. T.W. helped with crystallisation, data collection and data processing. R.N. performed the stability assays and pharmacological analyses on $A_{2A}R$–mini-G_S complexes. A.G.W.L. was involved in data processing and structure solution, refinement and analysis. Manuscript preparation was performed by B.C., A.G.W.L. and C.G.T. The overall project management was by C.G.T.

Author information. Co-ordinates and structure factors for the $A_{2A}R$–mini-G_S complex have been submitted to the PDB database under accession code 5G53.

Europe PMC Funders Author Manuscripts

structures are very similar and are thought to represent an active-intermediate conformation of the receptor, but not the fully active receptor that binds a G protein5. Observations that support this conclusion include the presence of rotamer changes of conserved amino acid residues associated with activation of other GPCRs18, and the absence of a large-scale movement of the cytoplasmic end of transmembrane helix 6 (H6) away from the receptor core12. The G protein-coupled state of $A_{2A}R$ exhibits higher binding affinity for agonists compared to the uncoupled state19, but it is unclear whether the agonist-bound structures determined so far depict the binding pocket in a high affinity or low affinity conformation. Therefore, in order to elucidate the structure of the activated state of $A_{2A}R$, we have determined its structure bound to a high-affinity agonist and an engineered G protein.

There is a single reported structure of a GPCR bound to a heterotrimeric G protein, namely G_s-bound β_2AR4, which showed that virtually all the atomic contacts between the receptor and G protein were formed by the Gα subunit. To facilitate the crystallisation of any GPCR-G_s complex, we developed a minimal G protein, mini-G_s, that comprised a truncated form of the GTPase domain of $G\alpha_s$ and included 8 point mutations to stabilise the protein in the absence of Gβγ and in the presence of detergents3. In addition, 3 truncations removed the switch III region, 25 amino acids from the N-terminus and the α-helical domain . Mini-G_s reproduced the increase in agonist affinity that occurred upon incubation of the receptor in the presence of the heterotrimeric G protein G_s and it also showed identical sensitivity to the presence of the allosteric antagonist Na^+ (Fig. 1 and Extended Data Fig. 1). In addition, mini-G_s readily formed a complex with $A_{2A}R$ in the presence of the agonist NECA and the complex was considerably more thermostable, particularly in short chain detergents, than $A_{2A}R$ with only NECA bound (Extended Data Fig. 2). This complex was crystallised in the detergent octylthioglucoside by vapour diffusion, a data set collected from two crystals, the structure determined by molecular replacement (see Online Methods) and refined to 3.4 Å (Extended Data Table 1). Of the two $A_{2A}R$–mini-G_s complexes per crystallographic asymmetric unit, the density in complex AC was better defined and was therefore used for all subsequent analyses below (see Supplementary Discussion).

The $A_{2A}R$–mini-G_s complex contained density for the agonist NECA bound to $A_{2A}R$ and density for a molecule of GDP bound to mini-G_s (Extended Data Fig. 3). The presence of GDP in the mini-G_s structure is a reflection of the properties of the engineered G protein, which, after complex formation, is insensitive to GTPγS-mediated dissociation3. Mini-Gs is in a conformation virtually identical to that observed in the β_2AR–Gs structure (see below) and therefore represents an active state of the G protein, consistent with its ability to couple to $A_{2A}R$ and induce high-affinity agonist binding (Fig. 1). The interface between $A_{2A}R$ and mini-G_s is formed between 20 amino acid residues from the receptor and 17 residues in mini-G_s (Fig. 2, Extended Data Figs. 4-6, Supplementary Table 1), comprising a total buried surface area of 1048 $Å^2$ on the receptor. In mini-G_s, contacts are made predominantly by the α5 helix involving 14 amino acid residues that pack against residues in H3, CL2, H5, H6, H7 and H8 of $A_{2A}R$. Additional interactions include residues in S1, S3, the S2-S3 loop and α5 that form a hydrophobic pocket in which the side chain Leu110 in CL2 of $A_{2A}R$ is sequestered (Extended Data Fig. 7). Amino acid residues in $A_{2A}R$ and mini-G_s form complementary surfaces that pack together predominantly via van der Waals interactions (~90% of contacts) with 6 polar interactions across the interface. Helix α5 protrudes into the

cleft within the cytoplasmic face of $A_{2A}R$ created through the outward bending of the cytoplasmic end of H6. The apex of the α5 helix, Tyr391$^{H5.23}$ (superscript refers to the CGN system for G proteins7) makes extensive van der Waals interactions with Arg102$^{3.50}$ (superscript refers to the Ballesteros-Weinstein numbering system for GPCRs20) that forms the whole upper surface of the cleft (Fig. 3).

Superposition of the receptors in the $A_{2A}R$–mini-G_s complex and the β_2AR–G_s complex4 shows that the receptors have very similar architectures (rmsd 1.7 Å over 1239 atoms). The intracellular faces of the receptors align very well, including the large outward shift of the cytoplasmic end of H6 on activation. However, mini-G_s does not superimpose exactly on the Gα subunit of the heterotrimeric G protein bound to β_2AR (Fig. 3). There is a difference in orientation of ~15°, although the difference is smaller (~10°) for the α5 helix. This is probably a consequence of the different amino acid residues in $A_{2A}R$ compared to β_2AR (Fig. 3 and Extended Data Fig. 5), which results in a slightly different packing of the G proteins to the receptors, although we cannot discount the possible influence of lattice contacts. Alignment of mini-G_s with $G\alpha_s$ bound to β_2AR shows that they are essentially identical (rmsd 0.92 Å over 1158 atoms), with the most significant difference being an 8° tilt between the respective α5 helices, resulting in a 3.7 Å displacement of the Cα of Tyr391 in mini-G_s away from the core of the G protein (Extended Data Fig. 8). Overall, there are 14 contacting residues in common between β_2AR and $A_{2A}R$ G_s complexes, with an additional 6 contacting residues present only in $A_{2A}R$ and another 10 present only in β_2AR (Supplementary Table 1). Many of the contacts between residues in the α5 helix of the G protein and the receptors are conserved, although the exact orientation and atomic contacts may differ (Fig. 3; Extended Data Fig 6, Supplementary Table 1). Similarly, there is a highly conserved interaction between a hydrophobic residue in the centre of CL2, Leu110 in $A_{2A}R$ and Phe139 in β_2AR, and residues His41$^{S1.2}$, Val217$^{S3.1}$ and Asp215$^{s2s3.1}$ in Gαs (Extended Data Fig. 7). The most significant difference between the $A_{2A}R$–mini-G_s interface compared to the β_2AR–G_s interface occurs as a result of the different amino acid sequences at the H7-H8 boundary. In $A_{2A}R$, H7 terminates with Arg291$^{7.56}$ and forms the sequence R$^{7.56}$IR*EF*R (amino acid residues in italics do not contact mini-G_s), compared to the sequence *S*$^{7.56}$*PDFRI* in the equivalent position of β_2AR, where none of the residues make contacts with $G\alpha_s$. Another region of the receptors that differs in the presence/absence of contacts to their respective G proteins is at the end of H5, due to the extension of H5 in β_2AR by an additional turn compared to $A_{2A}R$ (Fig. 3; Extended Data Fig 6, Supplementary Table 1). From these examples it is clear that although the majority of amino acid residues at the interface between the receptor and G protein are identical, the specific atoms involved in the contacts differ either in terms of the amino acid side chains involved, their relative dispositions at the interface and/or the nature of the interaction.

Comparison of the active-intermediate state of UK432097-bound $A_{2A}R6$ with the structure of $A_{2A}R$ bound to mini-G_s identified major re-arrangements in the cytoplasmic half of the receptor core to accommodate G protein binding (Fig. 4) and will be described in terms of the re-arrangements required to transition from the active-intermediate state to the activated G protein-bound conformation. Firstly, the cytoplasmic end of H6 moves away from the receptor core by 14 Å as measured between the Cα atoms of Thr224$^{6.26}$ in the two different conformations. This movement is achieved through H6 bending outwards with little

discernible rotation around the helix axis. The extent of H6 movement is dictated by van der Waals interactions between Lys227$^{6.29}$, Ala231$^{6.33}$ and Leu235$^{6.37}$ in $A_{2A}R$ and Leu393$^{H5.25}$ and the carboxy terminus of mini-G_s. The movement of H6 requires significant changes in the packing of the cytoplasmic end of H6 with helices H5 and H7. In particular, the side chains of highly conserved Tyr197$^{5.58}$ and Tyr288$^{7.53}$ both adopt new rotamers to fill the space previously occupied by the side chains of Leu235$^{6.37}$ (whose Cα moves by 3.7 Å) and Ile238$^{6.40}$ (Cα moves by 2.2 Å) respectively. The shift in Tyr288$^{7.53}$ allows Arg102$^{3.50}$ of the conserved DRY motif to adopt a fully extended conformation, packing against the side chain of Tyr391$^{H5.23}$ in the α5 helix of mini-G_s. It is striking that the structural change from the inactive conformation to the active-intermediate state5 is characterised by the concerted rotation of H5, H6 and H7, whereas the conformation change from the active-intermediate state to the active conformation upon mini-G_s binding is characterised by the bending of H6 with little further rotation. In contrast to the considerable re-arrangements of the cytoplasmic half of the receptor, there are no significant changes in the extracellular half of the receptor (Fig. 4; Extended Data Fig. 9). Thus the disposition of the ligand binding pocket described in the active-intermediate state most likely describes the high-affinity state of NECA-bound to $A_{2A}R$.

$A_{2A}R$ appears to have a very different energy landscape to the β-adrenergic receptors (βARs). Both $A_{2A}R$ and β_2AR exist in an ensemble of conformations whether bound to antagonists, agonists or to no ligand at all, and the presence of agonists increases the probability of formation of a fully active state21,22. This active state is then stabilised by binding of a G protein. Structures of βARs bound to agonists are all in a conformation very similar to the inactive state4,23–25, whereas structures of $A_{2A}R$ bound to agonists are in an active-intermediate state5,6,11 very similar to the active state. Whether there is an active-intermediate state for βARs equivalent to $A_{2A}R$ is unknown, but recently, it has been proposed based on extensive EPR data that β_2AR also exists in two distinct states in the active conformation21. The work here shows that the active-intermediate and fully active states are distinct conformations in the intracellular half of the receptor. Given the highly conserved nature of the mechanism of GPCR activation, it is likely that the active-intermediate of $A_{2A}R$ may represent a common intermediate for many Class A GPCRs, although it may exist only transiently depending on the energy landscape of the receptor.

Methods

Expression and purification of mini-G_s

The mini-G_s construct used (construct 414) was identical to mini-G_s (construct 393) previously described3, except that one additional mutation, L63Y, was included to improve crystal quality. An N-terminal histidine tag (His_6) and TEV protease cleavage site were present to facilitate purification. Mini-G_s was expressed in *E. coli* strain BL21(DE3)RIL upon induction with IPTG (50 μM) for 20 h at 25°C. Cells were harvested by centrifugation and lysed by sonication in lysis buffer (40 mM HEPES pH 7.5, 100 mM NaCl, 10% glycerol, 10 mM imidazole, 5 mM $MgCl_2$, 50 μM GDP, 1 mM PMSF, 2.5 μM Pepstatin-A, 10 μM Leupeptin, 50 μg/ml DNase I, 100 μg/ml lysozyme, 100 μM DTT), supplemented with Complete™ protease inhibitors (Roche). The lysate was clarified by centrifugation and

loaded onto a 10 ml Ni^{2+} Sepharose FF column. The column was washed with wash buffer (20 mM HEPES pH 7.5, 500 mM NaCl, 40 mM imidazole, 10% glycerol, 1 mM $MgCl_2$, 50 μM GDP) and eluted with elution buffer (20 mM HEPES pH 7.5, 100 mM NaCl, 500 mM imidazole, 10% glycerol, 1 mM $MgCl_2$, 50 μM GDP). TEV protease was added and the sample was dialysed overnight against dialysis buffer (20 mM HEPES pH 7.5, 100 mM NaCl, 10% glycerol, 1 mM $MgCl_2$, 10 μM GDP). TEV protease was removed by negative purification on Ni^{2+}-NTA resin (Qiagen). The sample was concentrated to 1.5 ml and loaded onto a Superdex-200 26/600 gel filtration column, equilibrated with gel filtration buffer (10 mM HEPES pH 7.5, 100 mM NaCl, 10% glycerol, 1 mM $MgCl_2$, 1 μM GDP, 0.1 mM TCEP). Peak fractions were pooled and concentrated to 100 mg/ml. The pure protein was aliquoted, flash-frozen in liquid nitrogen, and stored at -80°C. A typical yield was 100 mg of pure mini-G_s per litre of culture.

Expression and purification of adenosine $A_{2A}R$

Wild type human adenosine $A_{2A}R$ (residues 1-308) was modified to contain a C-terminal histidine tag (His_{10}) and TEV protease cleavage site. The N154A mutation was introduced to remove a potential N-linked glycosylation site. Recombinant baculoviruses expressing $A_{2A}R$ were prepared using the flashBAC ULTRA system (Oxford Expression Technologies). *Trichoplusia ni* cells were grown in suspension in ESF921 media (Expression Systems) to a density of $3x10^6$ cells/ml, infected with $A_{2A}R$ baculovirus and incubated for 72 h. Cells were harvested and membranes prepared by two ultracentrifugation steps in 20 mM HEPES pH7.5, 1 mM EDTA, 1mM PMSF. NECA (100 μM), NaCl (300 mM), PMSF (1mM) and Complete™ protease inhibitors (Roche) were added to the membranes, and the sample was mixed for 30 min at room temperature. Membranes from 3 L of cells were solubilised with 2% n-decyl-β-D-maltopyranoside (DM) on ice for 1 h. The sample was clarified by ultracentrifugation and loaded onto a 5 ml Ni-NTA column (Qiagen). The column was washed with wash buffer (20 mM HEPES pH 7.5, 500 mM NaCl, 10% glycerol, 80 mM imidazole, 100 μM NECA, 0.15% DM), and eluted with elution buffer (20 mM HEPES pH 7.5, 100 mM NaCl, 10% glycerol, 300 mM imidazole, 100 μM NECA, 0.15% DM). The eluate was concentrated using a 50 kDa cut-off Amicon centrifugal ultrafiltration unit (Millipore), and exchanged into desalting buffer (10 mM HEPES pH 7.5, 100 mM NaCl, 10% glycerol, 100 μM NECA, 0.15% DM) using a PD10 column (GE Healthcare). TEV protease was added, and the sample was incubated on ice overnight. TEV protease was removed by negative purification on Ni^{2+}-NTA resin. The sample was concentrated to 0.2 ml and loaded onto a Superdex 200 column (GE Healthcare). Peak fractions were pooled and concentrated to approximately 20 mg/ml. A typical yield was 2 mg of pure $A_{2A}R$ per litre of culture.

Complexation and crystallisation

Purified $A_{2A}R$ was mixed with a 1.2-fold molar excess of mini-G_s. $MgCl_2$ (1 mM) and apyrase (0.1 U) were added, and the mixture was incubated on ice overnight. The sample was diluted 10-fold in gel filtration buffer (10 mM HEPES pH 7.5, 100 mM NaCl, 100 μM NECA, 0.35% n-octyl-β-D-thioglucopyranoside OTG), concentrated to 0.2 ml, and loaded on to a Superdex 200 column (pre-equilibrated in the same buffer). Peak fractions, containing the $A_{2A}R$–mini-G_s complex, were pooled and concentrated to 20 mg/ml. The

$A_{2A}R$–mini-G_s complex was crystallised by vapour diffusion in OTG either in the presence or absence of cholesterol hemisuccinate (CHS), but there was no discernible difference in the quality of crystals that grew under the two different conditions (the structure was determined using data collected from 2 crystals, one from each condition). Crystallisation plates were set up at 4°C using 120 nl sitting drops. Crystals used for structure solution were grown in two conditions, either: 0.1 M NaOAc pH 5.5, 10% PEG 2000 (in the presence of CHS); or 0.1 M NaOAc pH 5.7, 9.5% PEG 2000 MME (in the absence of CHS). Crystals were cryo-protected in mother liquor supplemented with 30% PEG 400 and flash frozen in liquid nitrogen.

Data collection, processing and refinement

Diffraction data were collected at the European Synchrotron Radiation Facility on beamline ID23-2 with a Pilatus 2M detector, using a 6 μm x 8 μm microfocus beam (0.8729 Å wavelength). Data were collected using either standard or helical collection modes. Data from two crystals were used for structure solution. Data were processed using MOSFLM26 and AIMLESS27. The structure was solved by molecular replacement with PHASER28 using the structures of the thermostabilised $A_{2A}R$ (PDB ID: 2YDV)5 and the $G\alpha_s$ GTPase domain (residues 40-59 and 205-394) from the β_2AR–G_s complex (PDB ID: 3SN6)4 as search models. Model refinement and rebuilding were performed using REFMAC29 and COOT30.

Competition binding assay

FreeStyle HEK293-F cells transiently expressing wild type $A_{2A}R$ were resuspended in either assay buffer A (25 mM HEPES, pH 7.5, 100 mM KCl, 1 mM $MgCl_2$), assay buffer B (25 mM HEPES, pH 7.5, 100 mM NaCl, 1 mM $MgCl_2$), or assay buffer C (25 mM HEPES, pH 7.5, 500 mM NaCl, 1 mM $MgCl_2$), and were lysed by 10 passages through a 26-gauge needle. Purified binding partners were buffer-exchanged to the respective buffer before being added to the membranes at a final concentration of 25 μM. The mixture was aliquoted and NECA was added (0 to 1 mM final concentration, prepared in assay buffers containing 1 u/mL apyrase). The samples were incubated for 90 min at 22°C, ^{3}H-ZM241385 was added at its apparent K_d (2.5 nM) and allowed to bind for a further 90 min at 22°C. Non-specific binding was determined in the presence of 100 μM of ZM241385. Receptor-bound and free radioligand were separated by filtration through 96-well GF/B filter plates (pre-soaked with 0.1% polyethyleneimine), and washed 3 times with the appropriate buffer. Plates were dried and radioactivity was quantified by liquid scintillation counting using a Tri-Carb 2910 TR (Perkin Elmer). Data were analyzed by nonlinear regression using GraphPad Prism software. The K_i for NECA binding was derived from one-site fit K_i analysis. Data from at least three independent experiments, each performed in duplicate, were analyzed using an unpaired two-tailed t-test for statistical significance.

Thermostability assay

Membranes from *Trichoplusia ni* cells expressing wild type human $A_{2A}R$ were resuspended in T_m buffer (25 mM HEPES pH 7.5, 100 mM NaCl, 1 mM $MgCl_2$) and homogenised by 10 passages through a 26-gauge needle. Binding partner was added at a final concentration of 25 μM. ^{3}H-NECA and unlabelled NECA were mixed in a molar ratio of 1:5 and added to the

Europe PMC Funders Author Manuscripts

membranes to give a final concentration of 1 μM (approximately 10-fold above the apparent K_d). The samples were incubated at room temperature for 1 h, then chilled on ice for 30 min. DDM, DM or OG were added to a final concentration of 0.1%, 0.13% or 0.8%, respectively, and samples were incubated on ice for 1 h. Cell debris and insoluble material were removed by centrifugation for 5 min at 20,000 x*g* and the supernatant was aliquoted into PCR strips. Samples were heated to the desired temperature for exactly 30 min, then quenched on ice for 30 min. Samples (50 μl) were loaded onto gel filtration resin packed into a 96-well filter plate (Millipore), which was centrifuged to separate receptor-bound from free radioligand. Non-specific binding was determined in the presence of 200 μM unlabeled NECA. Radioactivity was quantified by liquid scintillation counting using a MicroBeta TriLux scintillation counter (PerkinElmer). Data were analyzed by nonlinear regression using GraphPad Prism software. Apparent T_m values were derived from sigmoidal dose-response analysis. Results represent the mean ± SEM of two independent experiments, performed in duplicate.

Europe PMC Funders Author Manuscripts

Extended Data

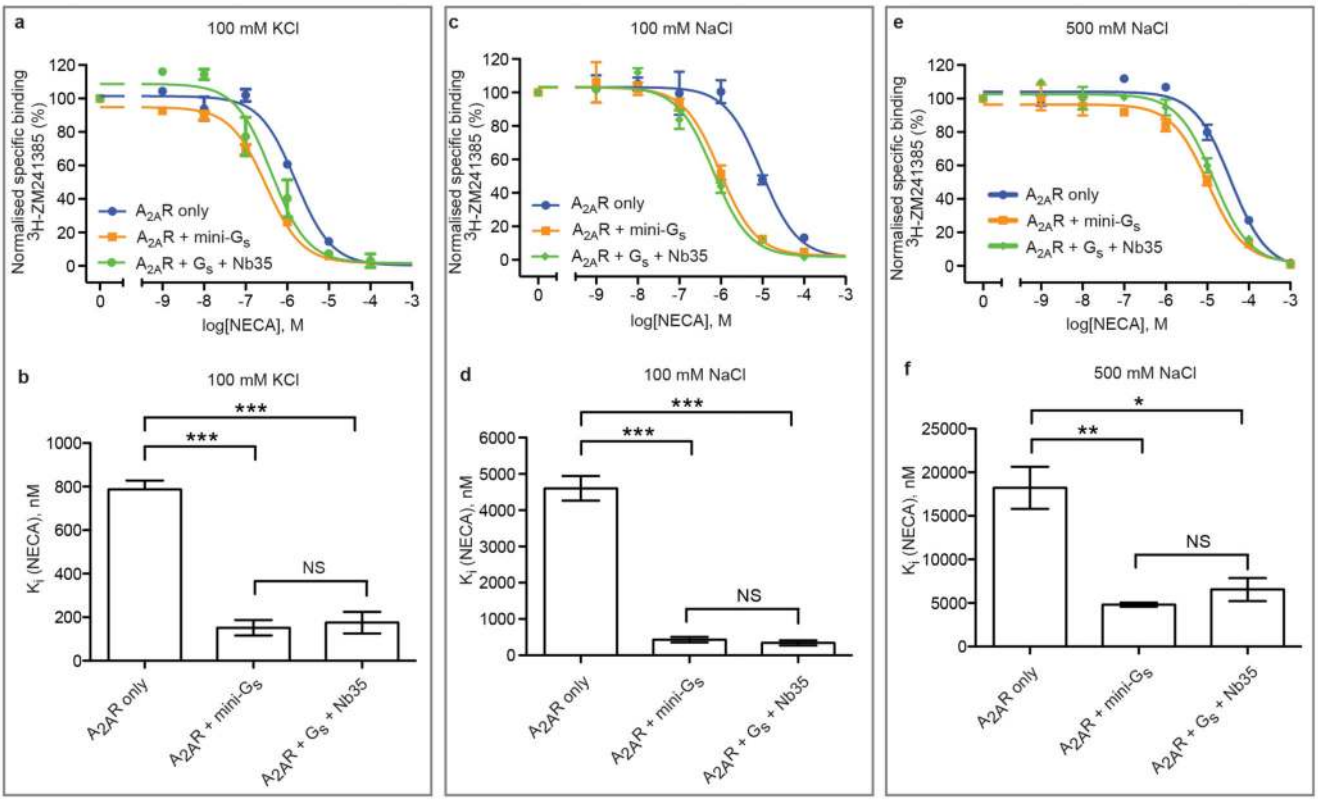

g

Salt type and concentration	K_i (NECA) ± SEM, nM		
	$A_{2A}R$	$A_{2A}R$ + mini-G_s	$A_{2A}R$ + G_s + Nb35
100 mM KCl	790 ±40	150 ± 40	180 ± 50
100 mM NaCl	4600 ± 340	430 ± 80	340 ± 70
500 mM NaCl	18200 ± 2400	4800 ± 230	6600 ± 1300

Extended Data Figure 1.

Pharmacological analyses of $A_{2A}R$–mini-Gs complexes. Competition assays were performed on $A_{2A}R$ expressed in HEK293 cell membranes with the agonist NECA competing for the binding of radiolabelled inverse agonist ^{3}H-ZM241385. Experiments were performed in the presence of either 100 mM KCl (**a**,**b**), 100 mM NaCl (**c**, **d**) or 500 mM NaCl (**e**, **f**) to confirm the similar behaviour of mini-Gs with heterotrimeric G_s with nanobody Nb35 for stabilisation of the complex. Results are summarised in the Table (**g**). Data from at least 3 independent experiments performed in duplicate were analysed with an unpaired t-test for statistical significance.

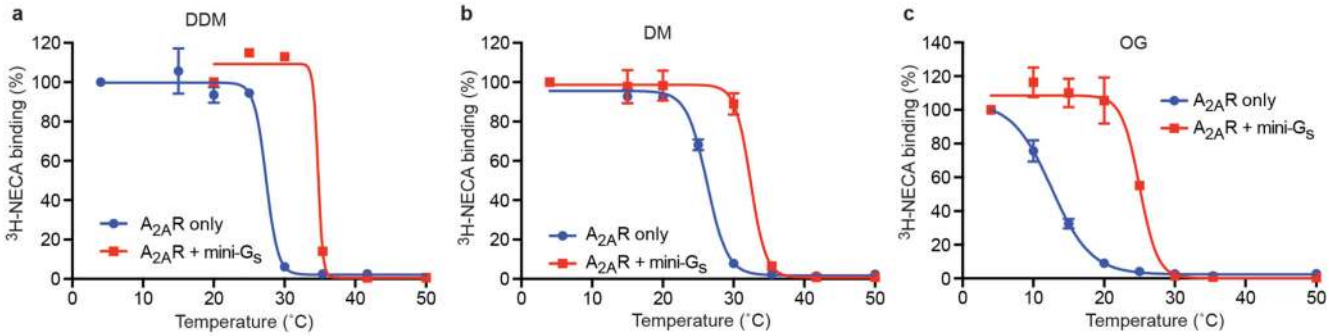

d

Detergent	A_{2A}R only	A_{2A}R + mini-G_s	ΔT_m (˚C)
Dodecylmaltoside (DDM)	27.0 ± 0.4 ˚C	34.2 ± 0.6 ˚C	7.2
Decylmaltoside (DM)	26.1 ± 0.1 ˚C	32.9 ± 0.5 ˚C	6.8
Octylglucoside (OG)	12.0 ± 0.6 ˚C	25.4 ± 0.3 ˚C	13.4

Extended Data Figure 2.

Thermostability of detergent-solubilised ^{3}H-NECA-bound A_{2A}R in the presence or absence of mini-Gs. Unpurified A_{2A}R was solubilised in detergent at the following concentrations: **a**, DDM, 0.1%; **b**, DM, 0.13%; **c**, OG, 0.8%. Samples were heated for 30 minutes, quenched on ice and the amount of ^{3}H-NECA bound determined. Data were analysed by non-linear regression and apparent T_m values were determined from analysis of the sigmoidal dose-response curves fitted (**d**). Results represent the mean ± SEM of two independent experiments, performed in duplicate.

Europe PMC Funders Author Manuscripts

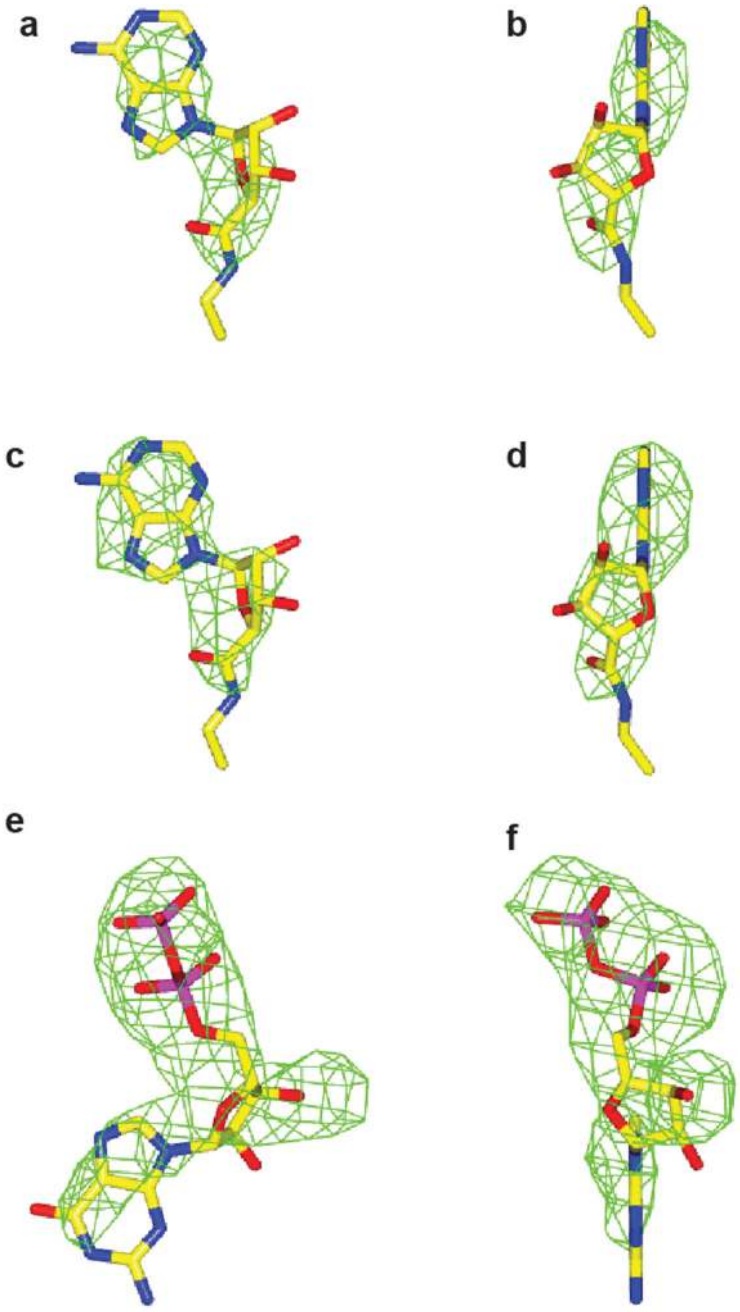

Extended Data Figure 3.

Omit maps for NECA and GDP. Orthogonal views of omit map difference density for NECA in $A_{2A}R$ chain A (**a**, **b**), NECA in $A_{2A}R$ chain B (**c**, **d**) and GDP in mini-Gs chain C (**e**, **f**). The contour level is 2.5 sigma in panels a-d and 3.0 sigma in panels e and f. Figures were made using CCP4mg31.

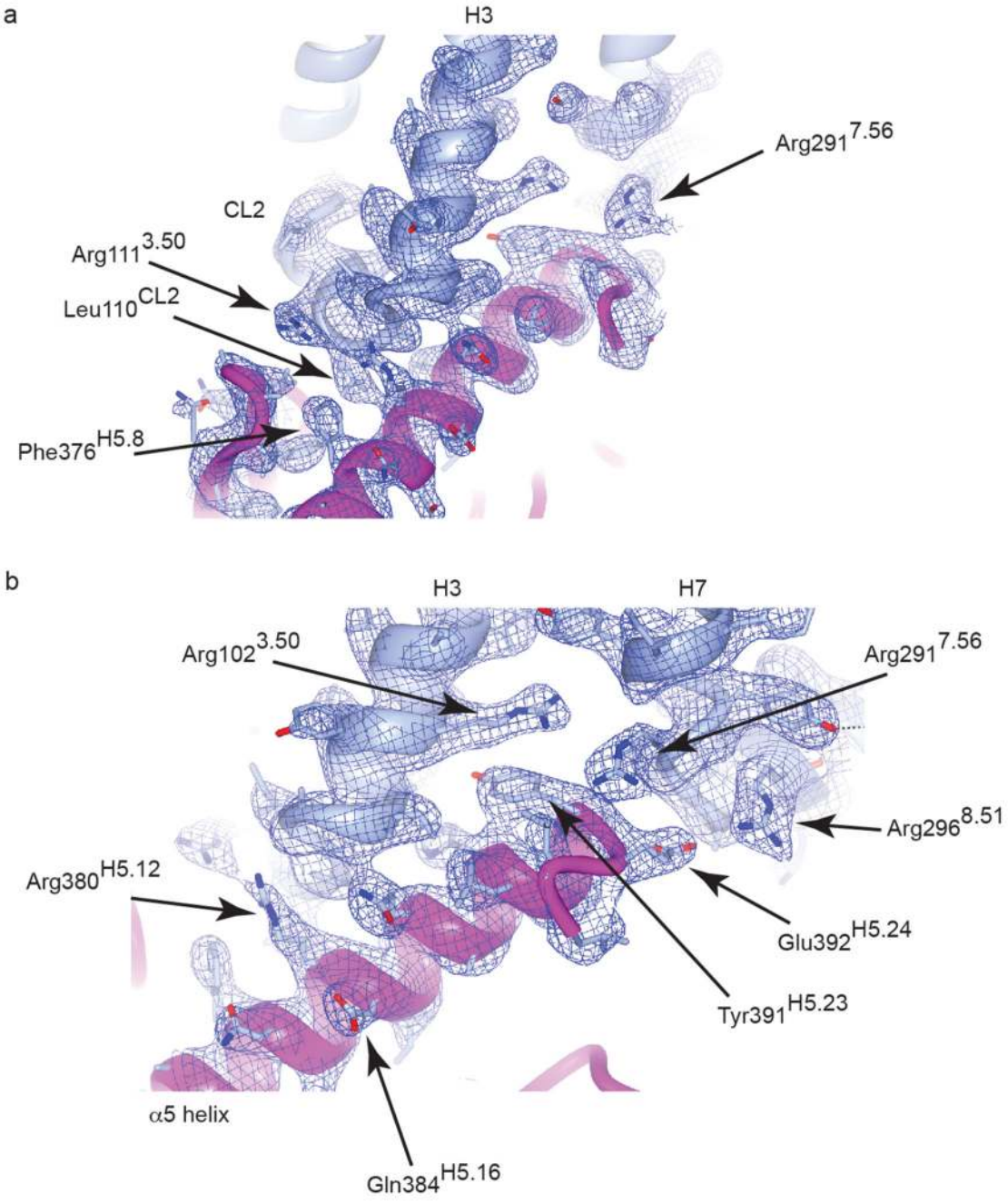

Extended Data Figure 4.

Electron density for the interface region of the $A_{2A}R$–mini G_s complex. The backbones of $A_{2A}R$ and mini-G_s are shown in cartoon representation in light blue and magenta respectively. Side chains are shown in stick representation (carbon, light blue; oxygen, red; nitrogen, deep blue). The electron density of the final 2Fo-Fc map is shown contoured at 1.2 sigma. For clarity, transmembrane helices H5 and H6 and the corresponding electron density have been omitted. (a) View showing the interaction between the C-terminal helix of mini-

G_s and the CL2 loop of $A_{2A}R$. (b) View showing the interactions between side chains of the C-terminal helix of mini-G_s and three Arg residues of $A_{2A}R$.

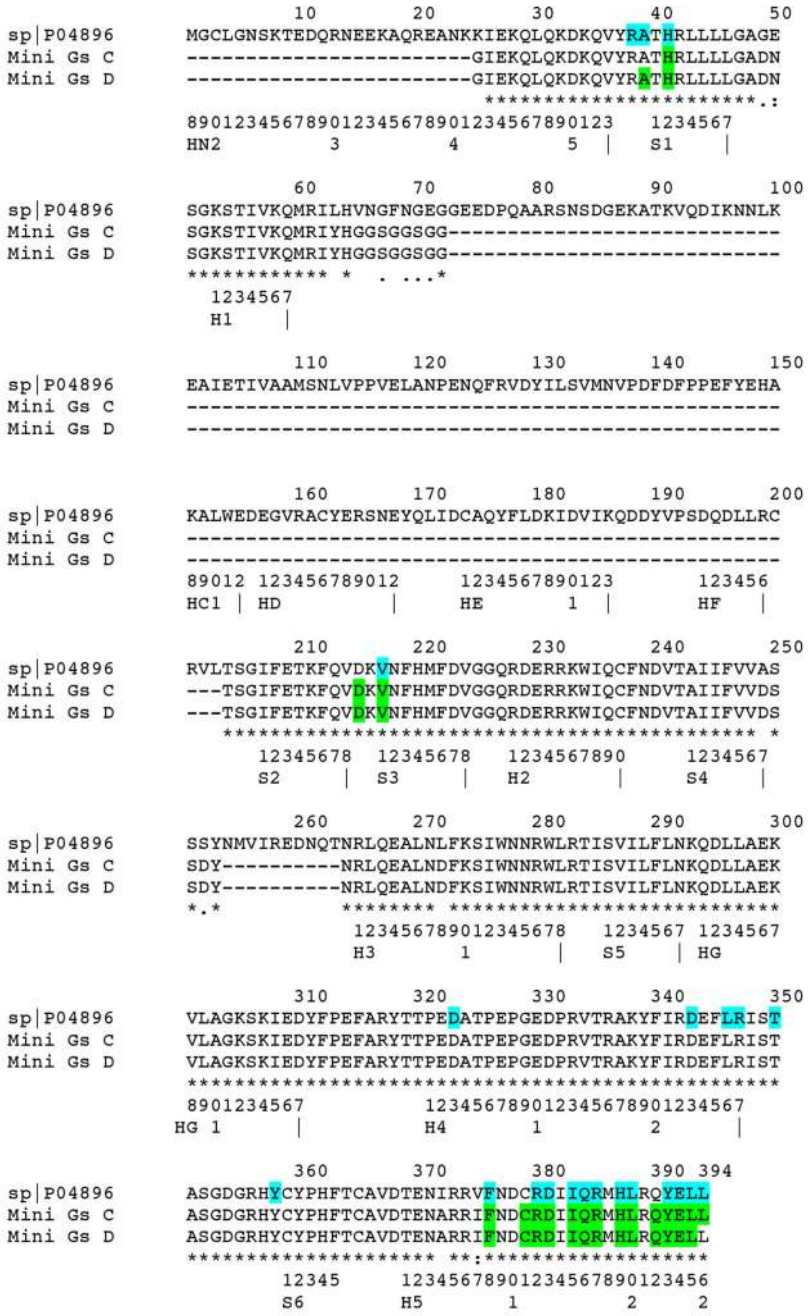

Extended Data Figure 5.

Alignment of mini-Gs with GNAS2. Comparison of amino acid residues in mini-G_s (chains C & D) within 3.9 Å of $A_{2A}R$ (green) in the $A_{2A}R$–mini-Gs structure and the amino acid residues in bovine GNAS2 (P04896) within 3.9 Å of β_2AR in the β_2AR–G_s structure (turquoise). The CGN system is used for reference.

Europe PMC Funders Author Manuscripts

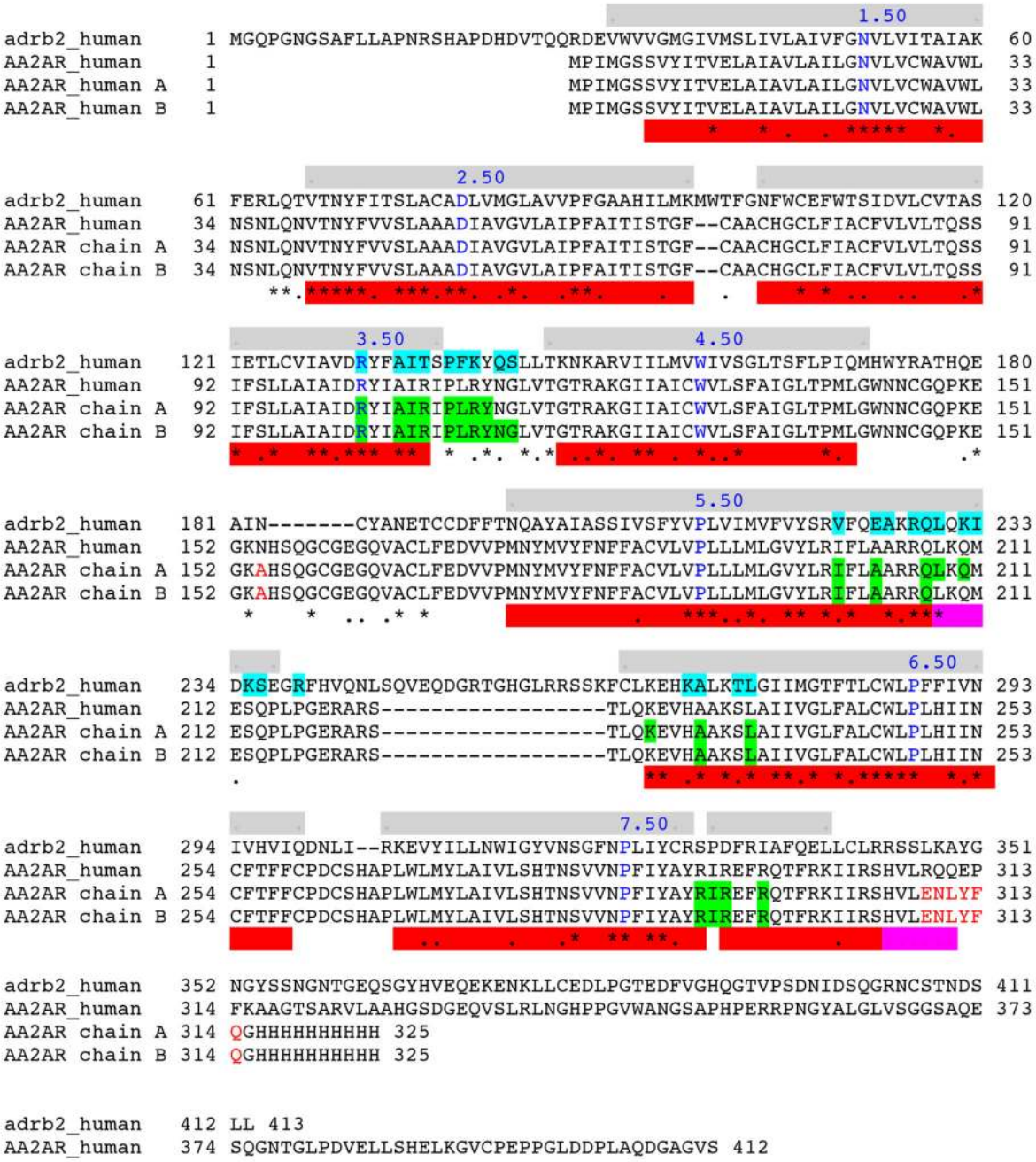

Extended Data Figure 6.

Alignment of β_2AR and A_{2A}R amino acid sequences. adrb2_human, human β_2-adrenergic receptor; AA2AR_human, human adenosine A_{2A} receptor; AA2AR chain A, chain A of the crystallised A_{2A}R–mini-G_s structure; AA2AR chain B, chain B of the crystallised A_{2A}R–mini-G_s structure. Residues in the receptors that are within 3.9 Å of either G_σ in the β_2AR–G_s complex or mini-G_s in the A_{2A}R–mini-G_s complex are highlighted in turquoise or green, respectively. Key Ballesteros-Weinstein numbers are shown in blue and mutations in the crystallised A_{2A}R to facilitate purification and crystallization are shown in red. Grey bars

Europe PMC Funders Author Manuscripts

indicate the positions of α-helices in the β_2AR–G_s structure, whereas red bars represent these regions in the A_{2A}R–mini-G_s structure; where there is a discrepancy in helix length between Chain A and B of A_{2A}R, the bar is coloured pink.

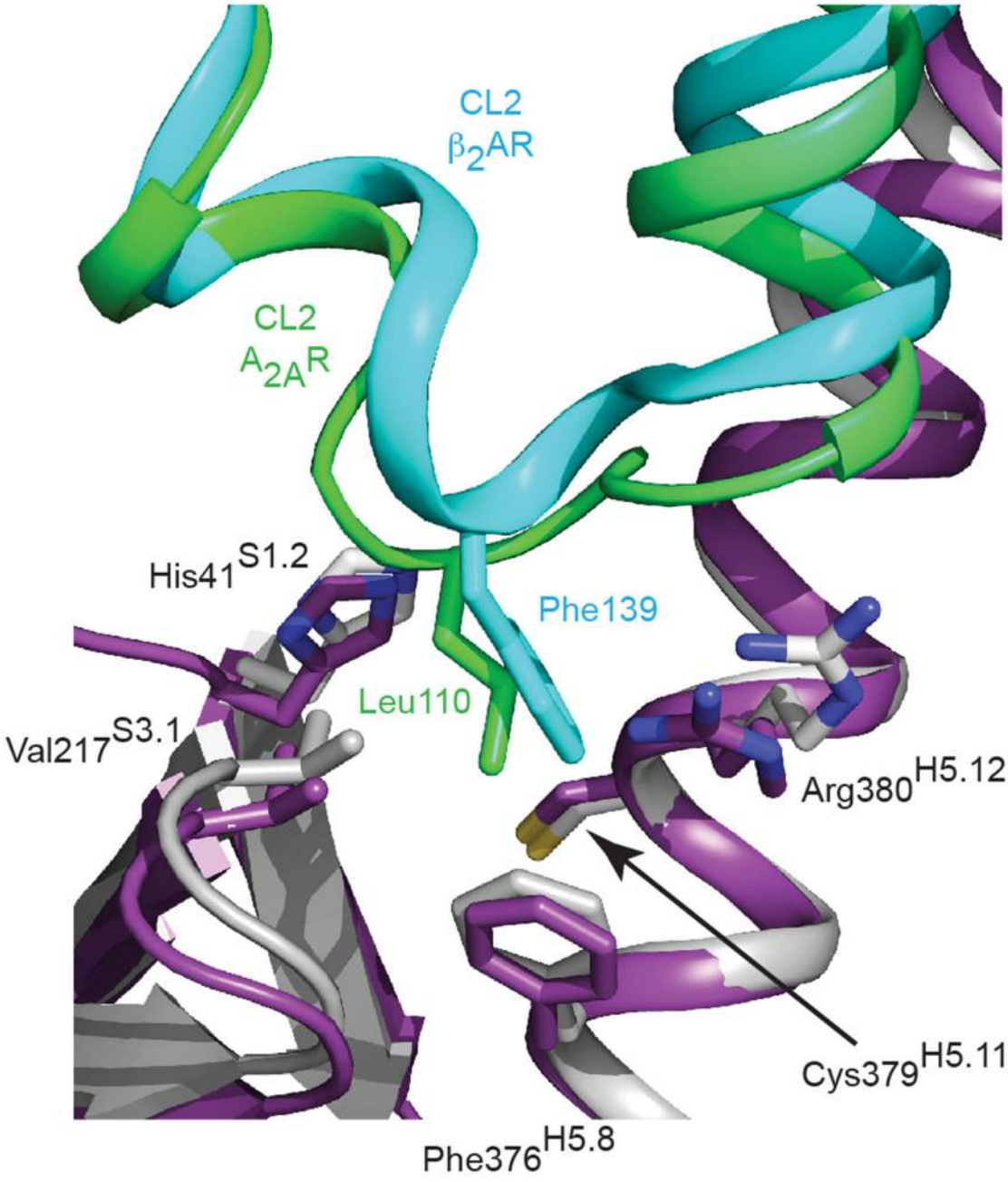

Extended Data Figure 7.

A conserved hydrophobic binding pocket at the receptor-Gα$_\sigma$ interface. The A_{2A}R–mini-G_s complex was aligned to the β_2AR–G_s complex via the receptors; A_{2A}R, green; β_2AR, turquoise; mini-G_s (purple); Gα$_s$ (grey).

Europe PMC Funders Author Manuscripts

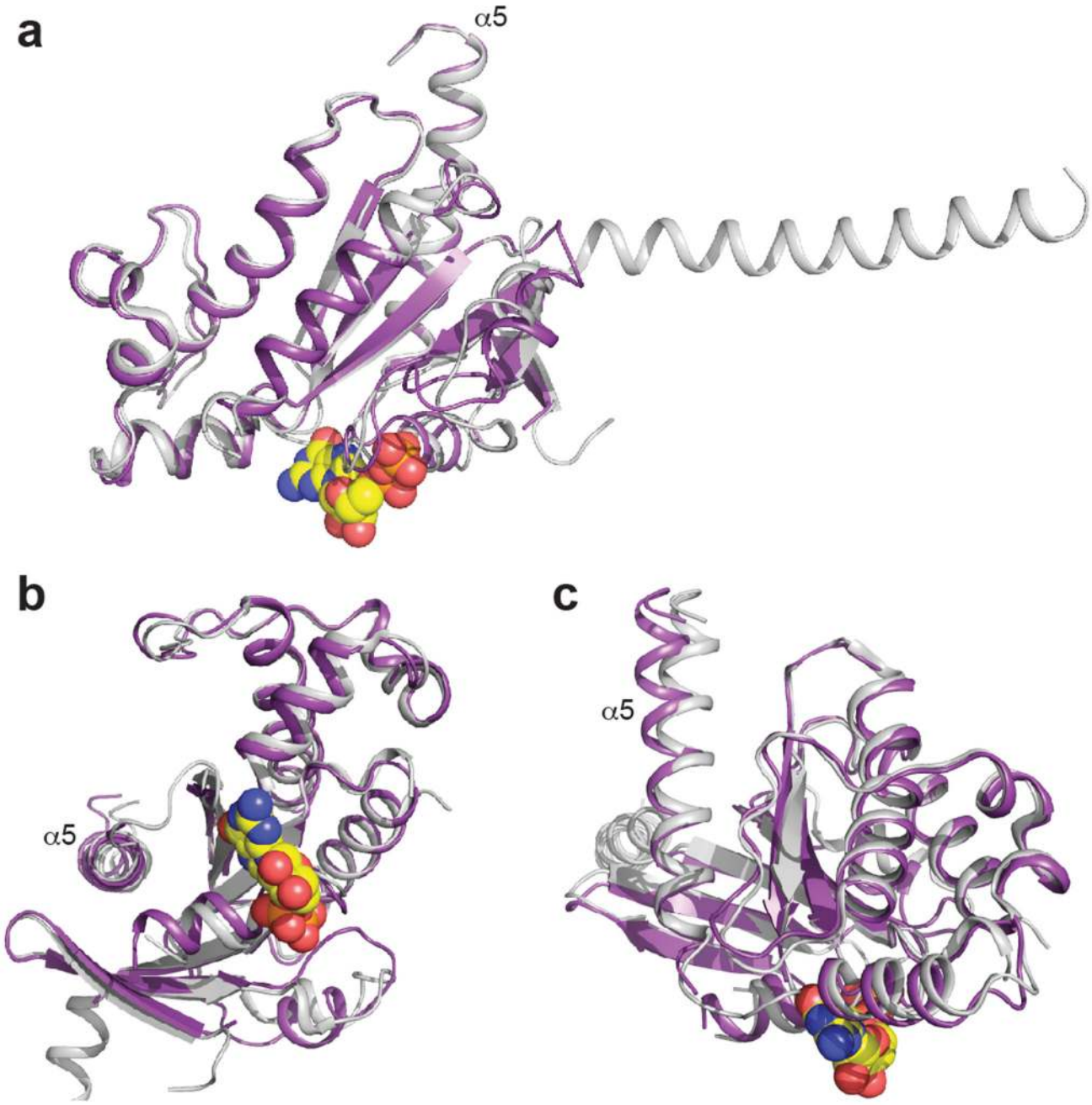

Extended Data Figure 8.

Comparison between receptor-bound mini-Gs and $G\alpha_{\sigma}$. **a-c**, Three different views of an alignment of mini-Gs (chain C, purple) bound to $A_{2A}R$ with the GTPase domain of $G\alpha_s$ (grey) bound to β_2AR. GDP bound to mini-Gs is depicted as a space filling model (carbon, yellow; oxygen, red; nitrogen, blue; phosphorus, orange). The α5 helix that interacts with the receptors is labelled.

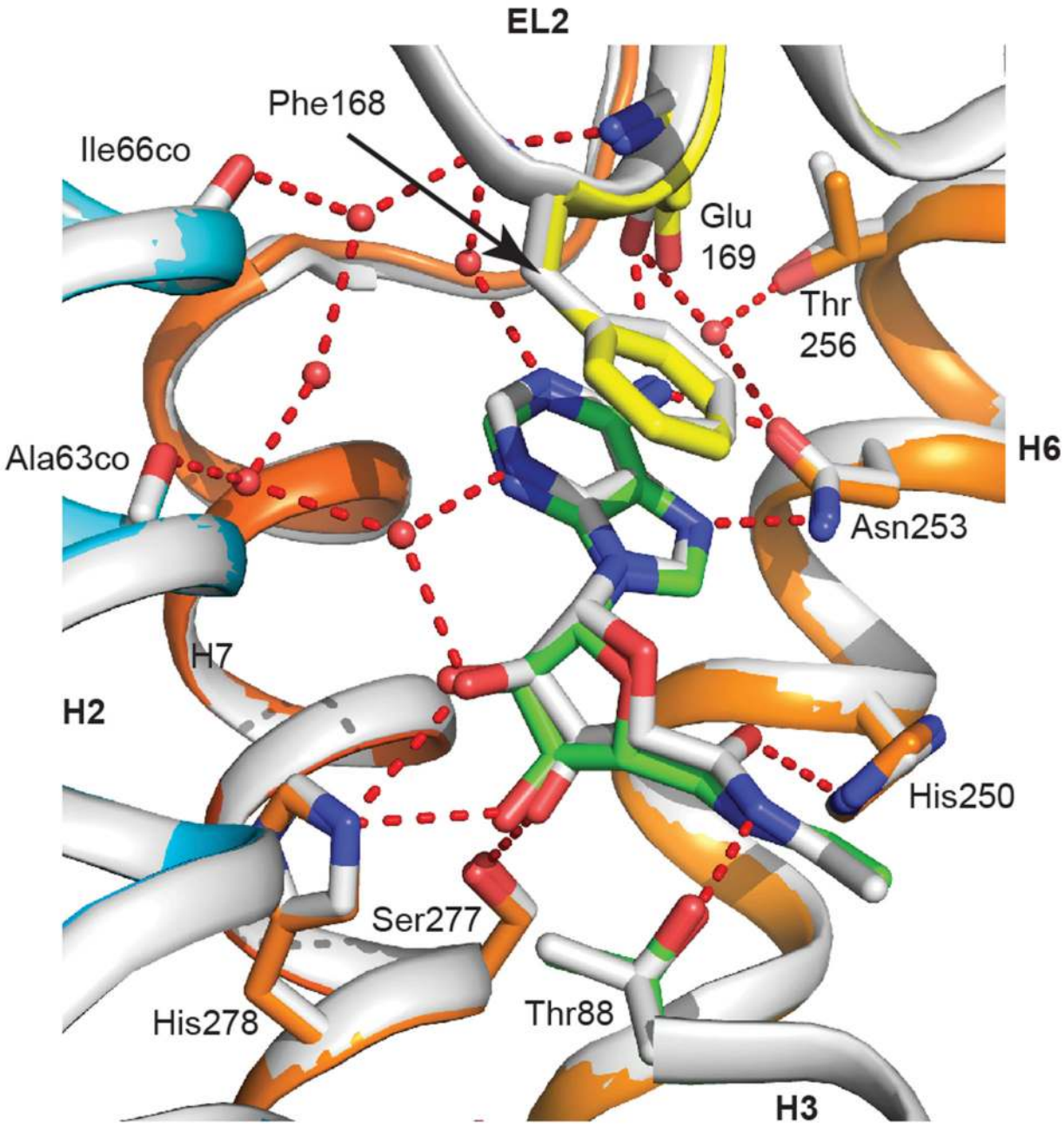

Extended Data Figure 9.

Comparison of the NECA binding site in the active-intermediate state compared to the mini-G_s-bound state. The structure of NECA-bound $A_{2A}R$ (grey cartoon, with the carbon atoms of NECA also in grey) in the active-intermediate state was aligned with the structure of the NECA-bound $A_{2A}R$–mini-G_s complex (rainbow colouration, with the carbon atoms of NECA in green). Key amino acid residues for both receptors are depicted (sticks; carbon atoms in the same colour as the respective receptor) that form hydrogen bonds (red dashed line) with either NECA or the associated water network (red spheres). Note that the water

molecules depicted are from only the NECA-bound $A_{2A}R$ structure in the active-intermediate state, because the resolution of the $A_{2A}R$–mini-G_s structure was insufficient to identify water molecules. Carbonyl oxygens are denoted by 'co' after the residue name.

Extended Data Table 1
Data collection and refinement statistics

Data Collection	
Space group	P 2_1 2_1 2_1
Cell dimensions *a*, *b*, *c* (Å)	90.6, 111.8, 161.3
Resolution (Å) [1]	40.3-3.4 (3.49-3.40)
R_{merge}	0.173 (0.747)
$I/\sigma I$	3.6 (1.2)
Completeness (%)	90.6 (78.5)
Redundancy	2.6 (2.4)
Refinement	
Resolution (Å)	40.3-3.4
No. reflections	19788
R_{work}/R_{free} %	28.4/31.5
No. atoms	7359
Protein	7248
Ligand/detergent/nucleotide	44/40/27
Water	0
B-factors (Å^2)	
Protein	79.9
Ligand/detergent/nucleotide	67.9/98.6/69.0
R.M.S.D.	
Bond lengths (Å)	0.008
Bond angles (°)	1.15

[1] Values in parentheses are for the highest resolution shell.

Supplementary Material

Refer to Web version on PubMed Central for supplementary material.

Acknowledgements

This work was supported by a grant from Heptares Therapeutics Ltd, the ERC (grant EMPSI 339995) and core funding from the Medical Research Council (MC_U105197215 and MC_U105184325). We thank the beamline staff at the European Synchrotron Radiation Facility (beamlines ID23-2, ID30-A3 and ID29) and at Diamond Light Source (beamline I24). We also thank R. Henderson, A. Jazayeri and T. Flock for comments on the manuscript. We declare a competing financial interest: this work was funded in part by Heptares Therapeutics Ltd. CGT is a consulatnat and member of the Scientific Advisory Board for Heptares Therapeutics Ltd.

References

1. Kobilka BK. Structural insights into adrenergic receptor function and pharmacology. Trends Pharmacol Sci. 2011; 32:213–218. [PubMed: 21414670]
2. Venkatakrishnan AJ, et al. Molecular signatures of G-protein-coupled receptors. Nature. 2013; 494:185–194. [PubMed: 23407534]
3. Carpenter B, Tate CG. Engineering a minimal G Protein to facilitate crystallisation of G protein coupled receptors in their active conformation. 2016 Submitted.
4. Rasmussen SG, et al. Crystal structure of the beta2 adrenergic receptor-Gs protein complex. Nature. 2011; 477:549–555. [PubMed: 21772288]
5. Lebon G, et al. Agonist-bound adenosine A2A receptor structures reveal common features of GPCR activation. Nature. 2011; 474:521–525. [PubMed: 21593763]
6. Xu F, et al. Structure of an agonist-bound human A2A adenosine receptor. Science. 2011; 332:322–327. [PubMed: 21393508]
7. Flock T, et al. Universal allosteric mechanism for Galpha activation by GPCRs. Nature. 2015; 524:173–179. [PubMed: 26147082]
8. Dore AS, et al. Structure of the adenosine A(2A) receptor in complex with ZM241385 and the xanthines XAC and caffeine. Structure. 2011; 19:1283–1293. [PubMed: 21885291]
9. Hino T, et al. G-protein-coupled receptor inactivation by an allosteric inverse-agonist antibody. Nature. 2012; 482:237–240. [PubMed: 22286059]
10. Jaakola VP, et al. The 2.6 angstrom crystal structure of a human A2A adenosine receptor bound to an antagonist. Science. 2008; 322:1211–1217. [PubMed: 18832607]
11. Lebon G, Edwards PC, Leslie AG, Tate CG. Molecular Determinants of CGS21680 Binding to the Human Adenosine A2A Receptor. Mol Pharmacol. 2015; 87:907–915. [PubMed: 25762024]
12. Lebon G, Warne T, Tate CG. Agonist-bound structures of G protein-coupled receptors. Current opinion in structural biology. 2012
13. Congreve M, et al. Discovery of 1,2,4-triazine derivatives as adenosine A(2A) antagonists using structure based drug design. Journal of medicinal chemistry. 2012; 55:1898–1903. [PubMed: 22220592]
14. Liu W, et al. Structural basis for allosteric regulation of GPCRs by sodium ions. Science. 2012; 337:232–236. [PubMed: 22798613]
15. Miller-Gallacher JL, et al. The 2.1 A resolution structure of cyanopindolol-bound beta1-adrenoceptor identifies an intramembrane Na+ ion that stabilises the ligand-free receptor. PLoS One. 2014; 9:e92727. [PubMed: 24663151]
16. Fenalti G, et al. Molecular control of delta-opioid receptor signalling. Nature. 2014; 506:191–196. [PubMed: 24413399]
17. Zhang C, et al. High-resolution crystal structure of human protease-activated receptor 1. Nature. 2012; 492:387–392. [PubMed: 23222541]
18. Huang W, et al. Structural insights into micro-opioid receptor activation. Nature. 2015; 524:315–321. [PubMed: 26245379]
19. Murphree LJ, Marshall MA, Rieger JM, MacDonald TL, Linden J. Human A(2A) adenosine receptors: high-affinity agonist binding to receptor-G protein complexes containing Gbeta(4). Mol Pharmacol. 2002; 61:455–462. [PubMed: 11809871]
20. Ballesteros, JA.; Weinstein, H. Integrated methods for the construction of three dimensional models and computational probing of structure function relations in G protein-coupled receptors. Methods in Neurosciences. Sealfon, SC.; Conn, PM., editors. Vol. 25. Academic Press; San Diego, CA: 1995. p. 366-428.
21. Manglik A, et al. Structural Insights into the Dynamic Process of beta2-Adrenergic Receptor Signaling. Cell. 2015; 161:1101–1111. [PubMed: 25981665]
22. Ye L, Van Eps N, Zimmer M, Ernst OP, Prosser RS. Activation of the A2A adenosine G-protein-coupled receptor by conformational selection. Nature. 2016; 533:265–268. [PubMed: 27144352]
23. Rasmussen SG, et al. Structure of a nanobody-stabilized active state of the beta(2) adrenoceptor. Nature. 2011; 469:175–180. [PubMed: 21228869]

24. Rosenbaum DM, et al. Structure and function of an irreversible agonist-beta(2) adrenoceptor complex. Nature. 2011; 469:236–240. [PubMed: 21228876]
25. Warne T, et al. The structural basis for agonist and partial agonist action on a beta(1)-adrenergic receptor. Nature. 2011; 469:241–244. [PubMed: 21228877]
26. Leslie AG. The integration of macromolecular diffraction data. Acta Crystallogr D Biol Crystallogr. 2006; 62:48–57. [PubMed: 16369093]
27. Evans P. Scaling and assessment of data quality. Acta Crystallogr D Biol Crystallogr. 2006; 62:72–82. [PubMed: 16369096]
28. McCoy AJ, et al. Phaser crystallographic software. J Appl Crystallogr. 2007; 40:658–674. [PubMed: 19461840]
29. Murshudov GN, et al. REFMAC5 for the refinement of macromolecular crystal structures. Acta Crystallogr D Biol Crystallogr. 2011; 67:355–367. [PubMed: 21460454]
30. Emsley P, Lohkamp B, Scott WG, Cowtan K. Features and development of Coot. Acta Crystallogr D Biol Crystallogr. 2010; 66:486–501. [PubMed: 20383002]
31. Potterton L, et al. Developments in the CCP4 molecular-graphics project. Acta Crystallogr D Biol Crystallogr. 2004; 60:2288–2294. [PubMed: 15572783]
32. Winn MD, et al. Overview of the CCP4 suite and current developments. Acta Crystallogr D Biol Crystallogr. 2011; 67:235–242. [PubMed: 21460441]

Europe PMC Funders Author Manuscripts

Europe PMC Funders Author Manuscripts

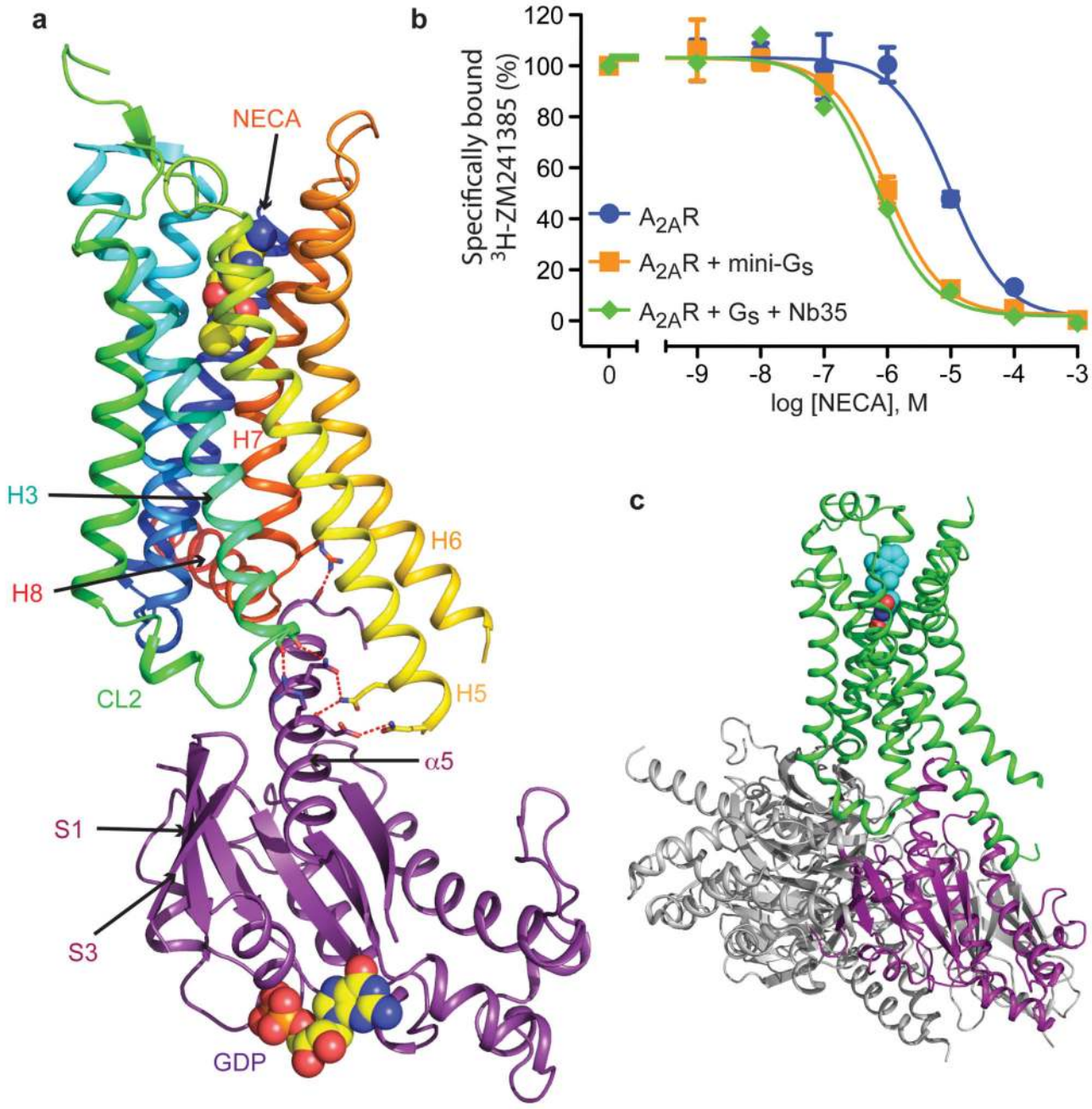

Figure 1.

Ligand binding and overall structure of the $A_{2A}R$–mini-G_s complex. **a**, The structure of $A_{2A}R$ is depicted as a cartoon in rainbow coloration (N-terminus in blue, C-terminus in red) with mini-G_s in purple. The agonist NECA bound to $A_{2A}R$ and GDP bound to mini-G_s are depicted as space-filling models (carbon, yellow; nitrogen, blue; oxygen, red; phosphorous, orange). Relevant secondary structural features are labelled. **b**, Mini-G_s increases the affinity of agonist binding to $A_{2A}R$ similar to that observed by a heterotrimeric G protein. Competition binding curves were performed in duplicate (n = 3) by measuring the

displacement of the inverse agonist ^{3}H-ZM241385 with increasing concentrations of the agonist NECA (K_i values in parentheses, see Extended Data Fig. 1 for full data): blue circles, $A_{2A}R$ (K_i 4.6 ± 0.3 μM); orange squares, $A_{2A}R$ and mini-G_s (K_i 430 ± 80 nM); green diamonds, $A_{2A}R$ and heterotrimeric G protein with nanobody Nb35 (K_i 340 ± 70 nM). G proteins were all added to membranes containing $A_{2A}R$ to give a final concentration of 25 μM and the final concentration of NaCl was 100 mM (see Methods online). **c**, The structure of β_2AR (green) bound to G_s (grey and purple) is depicted as a cartoon in the same orientation as $A_{2A}R$ in **a**; the purple region in G_s corresponds to the structure of mini-G_s.

Europe PMC Funders Author Manuscripts

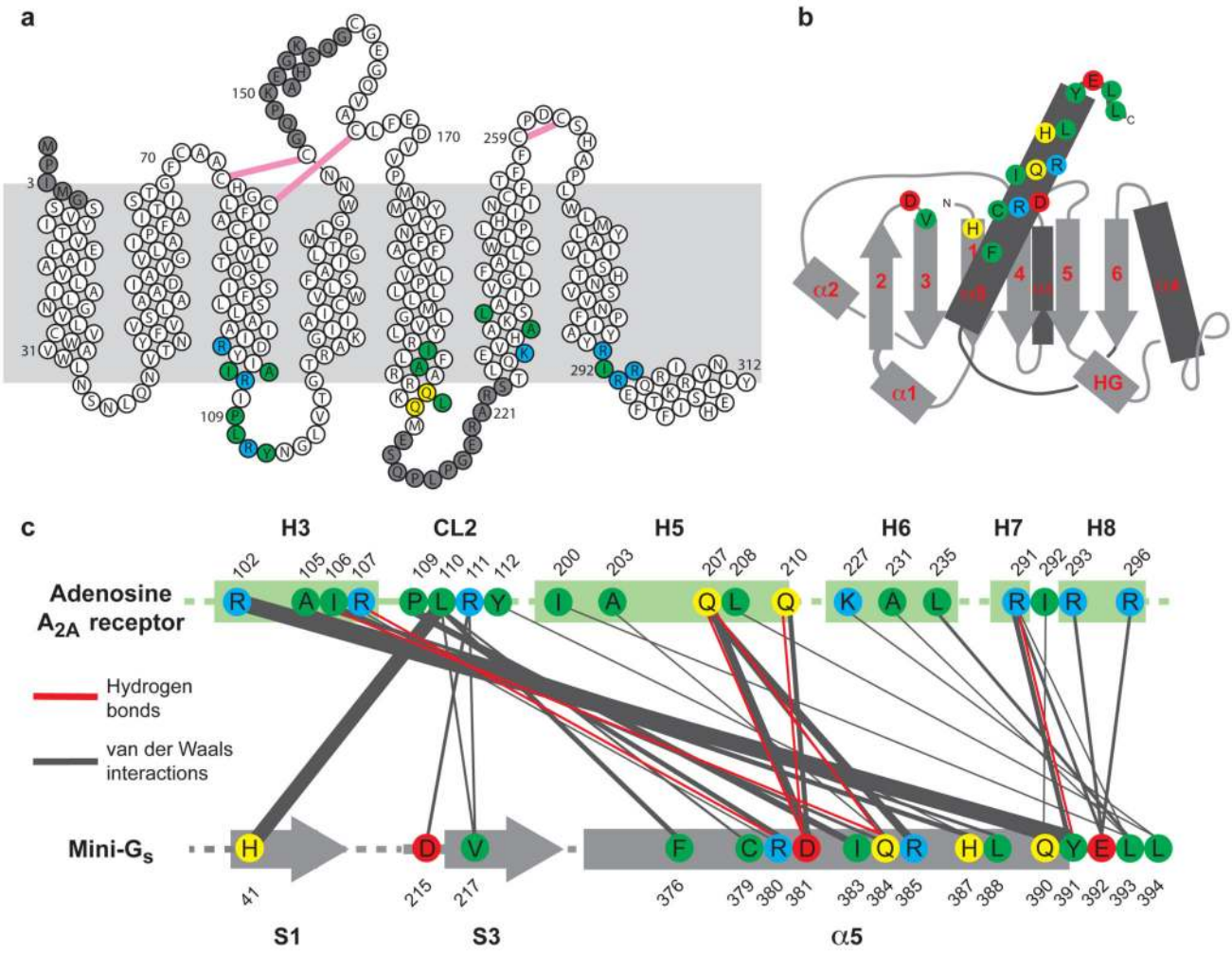

Figure 2.

Packing interactions between $A_{2A}R$ and mini-G_s. **a**, Diagram of $A_{2A}R$ depicting its secondary structure in the $A_{2A}R$–mini-G_s structure. Residues shaded in grey are disordered in either chain A and/or chain B. Disulphide bonds are depicted as pink lines. **b**, Cartoon of the mini-G_s topology. **c**, Diagram of contacts between mini-G_s and $A_{2A}R$, with line thickness representing the relative number of interactions between amino acid residues. In all panels, amino acid residues depicted in colour are at the interface between mini-G_s and $A_{2A}R$ (within 3.9 Å), with colours reflecting the properties of the side chain; blue, positively charged; red; negatively charged; green, hydrophobic; yellow, hydrophilic.

Europe PMC Funders Author Manuscripts

Europe PMC Funders Author Manuscripts

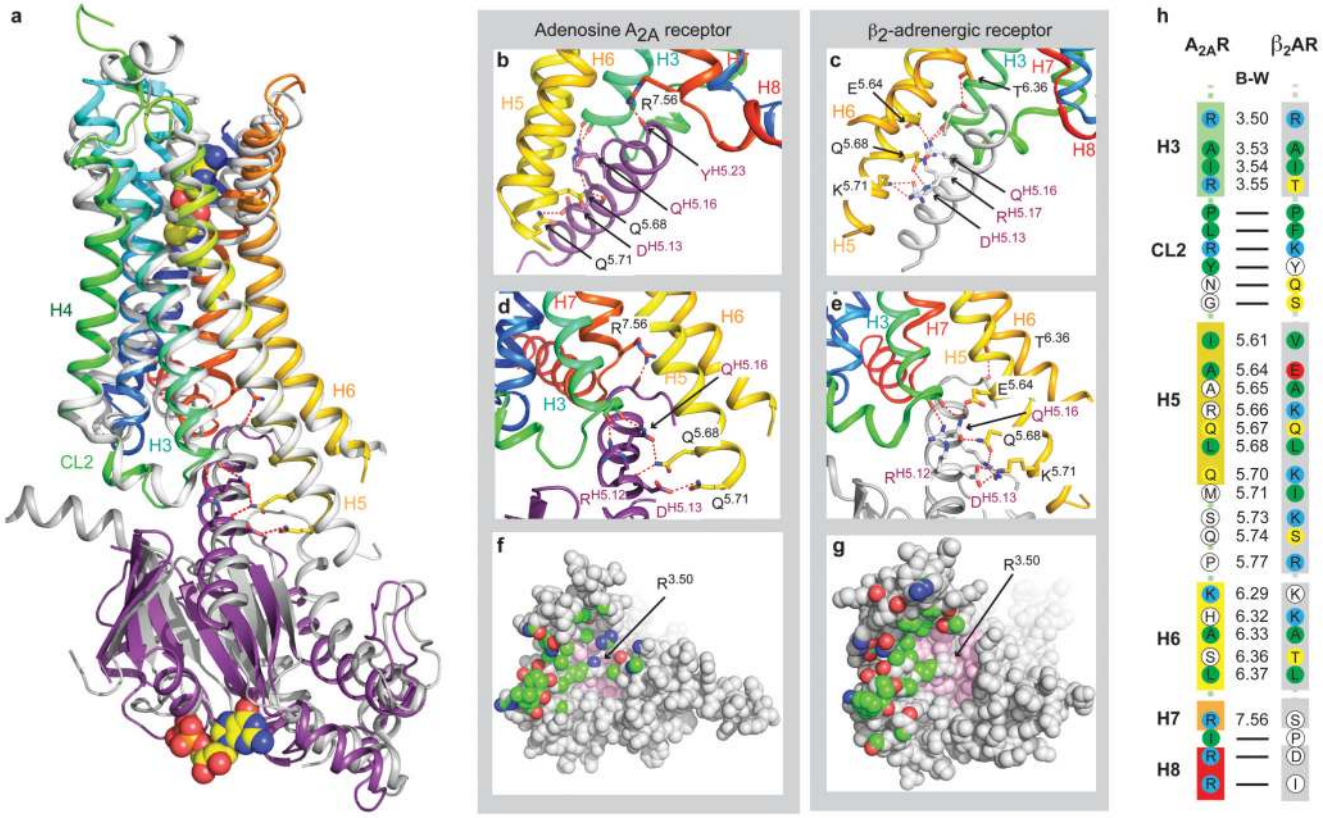

Figure 3.

Comparison of the $A_{2A}R$–mini-G_s and β_2AR–G_s complexes. **a**, Structural alignment of β_2AR–G_s (PDB ID: 3SN6)4 and $A_{2A}R$–mini-G_s was performed by aligning the receptors alone; $A_{2A}R$, rainbow colouration; β_2AR, grey. The resultant relative dispositions of $G\alpha_s$ (dark grey) bound to β_2AR and mini-G_s bound to $A_{2A}R$ (purple) are depicted. NECA and GDP are depicted as space-filling models (carbon, yellow; nitrogen, blue; oxygen, red; phosphorous, orange). The α-helical domain of $G\alpha_s$, $G\beta\gamma$ and Nb35 have all been omitted for clarity. **b**-**e**, Detailed comparisons of hydrogen bonds (red dashed lines) between the respective G proteins and receptors; both receptors are in rainbow colouration, with mini-G_s in purple and $G\alpha_s$ in grey. Labelling of amino acid residues shows the Ballesteros-Weinstein (B-W) numbers for the receptors and the CGN notation for G proteins. **f** and **g**, Views of the cytoplasmic surface of $A_{2A}R$ and β_2AR, respectively, as space-filling models with atoms making contacts with their respective G proteins coloured according to their type; carbon, green; nitrogen, blue; oxygen, red. Atoms coloured pink comprise conserved hydrophobic residues in the core of the receptors against which $Arg^{3.50}$ packs. **h**, Comparison of residues making contacts to G proteins in the $A_{2A}R$–mini-G_s complex and the β_2AR–G_s complex. Amino acid residues in the receptors that make contacts are coloured: red, negatively charged; blue, positively charged; green, hydrophobic; yellow, hydrophilic. Residues in white are those that do not make contact to the respective G protein, but the equivalent residue in the other receptor does. B-W numbers are given for residues in transmembrane α-helices, with a dash for residues in loops or H8. Amino acid residues 5.71-5.77 are disordered in the $A_{2A}R$–mini-G_s structure.

Europe PMC Funders Author Manuscripts

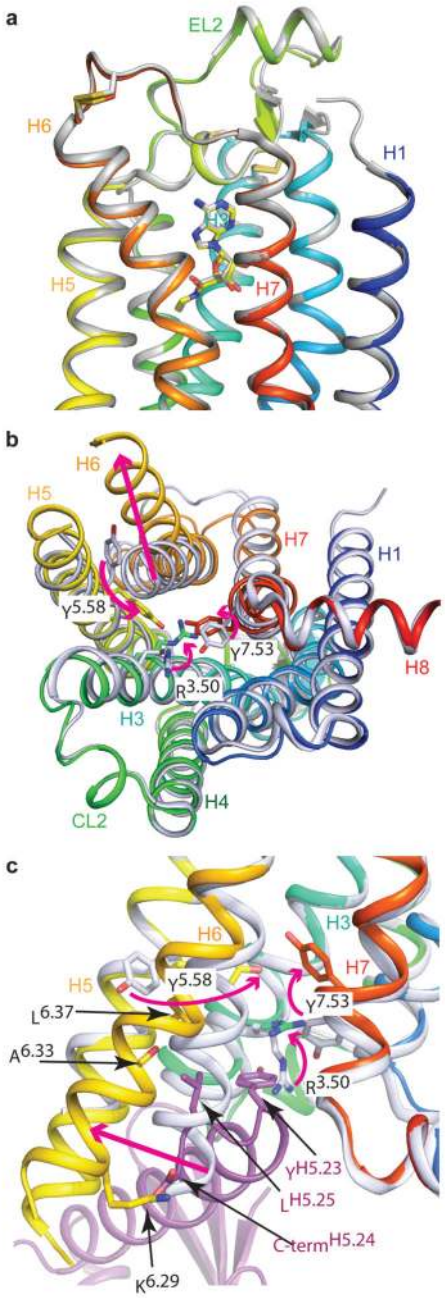

Figure 4.

Conformational changes in $A_{2A}R$ upon G protein binding. $A_{2A}R$ (rainbow colouration) bound to mini-G_s (purple) was aligned with $A_{2A}R$ in the active-intermediate conformation bound to either NECA (PDB ID: 2YDV)5 or UK432097 (PDB ID: 3QAK)6 to highlight structural changes upon G protein binding. Neither structure was used for both comparisons because the large extensions of the ligand UK432097 compared to NECA distorts the extracellular surface in comparison to the NECA-bound structure and the NECA-bound structure contains a thermostabilising mutation in the intracellular half of the receptor. **a**,

Alignment between 2YDV and the extracellular half of the $A_{2A}R$–mini-G_s complex is viewed parallel to the membrane plane. **b**, Alignment with 3QAK and viewed from the cytoplasmic surface with mini-G_s removed for clarity. **c**, Alignment with 3QAK viewed parallel to the membrane with the cytoplasmic side at the bottom. Residues are labelled with their Ballesteros-Weinstein numbers and arrows depict the direction of movement upon mini-G_s binding. Conversion of B-W and CGN numbers to amino acid residues in $A_{2A}R$ and mini-G_s, respectively, are as follows: $R^{3.50}$, Arg102; $Y^{5.58}$, Tyr197; $K^{6.29}$, Lys227; $A^{6.33}$, Ala231 carbonyl; $L^{6.37}$, Leu235; $Y^{7.53}$, Tyr288; $Y^{H5.23}$, Tyr391; $L^{H5.25}$, Leu393; C-term$^{H5.26}$, C-terminus of mini-G_s (Leu394). The receptor is in rainbow colours and the mini-G_s is in purple.